Fluid phase stability and equilibrium calculations in binary mixtures – Part I: Theoretical development for non-azeotropic mixtures

A. Giovanoglou, A. Galindo, G. Jackson and C.S. Adjiman[*]

Department of Chemical Engineering,

Centre for Process Systems Engineering

Imperial College London, South Kensington Campus

London SW7 2AZ, United Kingdom.

August 12, 2008

[*]Email: c.adjiman@imperial.ac.uk; Tel: +44 (0)207 594 6638

Abstract

A framework is proposed for the solution of fluid phase equilibrium ($P-T$ flash) for binary mixtures described by equations of state of general form. The framework is based on decomposing the phase equilibrium problem into sub-problems with more convenient and tractable mathematical and numerical properties. Systematic procedures are used to identify the mapping of the problem in the density and composition space, referred to as the density-composition pattern, at specified temperature and pressure. A series of stability tests is then carried out to explore the existence or non-existence of phases. Once the existence of a phase has been determined, the limits of stability and physical bounds on the problem are used to define the search area for that phase in the density-composition pattern. Finally, all available information from this detailed analysis is used for the solution of phase equilibrium between the phases identified in order to find the stable state at the specified conditions. The features of the proposed approach are exposed in detail through an algorithm for the fluid phase equilibria of the augmented van der Waals equation of state applied to non-azeotropic mixtures.

1   Introduction

The phase equilibrium problem consists in determining, for a given fluid mixture at specified conditions (usually pressure P, temperature T and total composition $\underline{z}$; i.e., the P-T flash), the number of equilibrium phases, their compositions and densities. There are two main approaches to formulate the phase equilibrium problem which can be derived from the restrictions that must hold at every stable equilibrium state as described by Baker *et al.* [1].

The first approach is based on the fact that a system is stable if and only if it attains the global maximum in the overall entropy or equivalently the global minimum in its free energy. These are the *necessary and sufficient* conditions for equilibrium, which in the case of a P-T flash at pressure P_{spec} and temperature T_{spec} can be cast as the following optimization problem

$$
\begin{aligned}
\min \quad & G_T \\
s.t. \quad & G_T = \sum_{k=1}^{np} \sum_{i=1}^{nc} n_{i,k} \mu_{i,k} \left(T_{spec}, \rho_k, n_{1,k}, \ldots, n_{nc,k}\right) \\
& P_{spec} = P_k \left(T_{spec}, \rho_k, n_{1,k}, \ldots, n_{nc,k}\right) && \forall k = 1, \ldots, np \\
& \sum_{k=1}^{np} n_{i,k} = N_i && \forall i = 1, \ldots, nc \\
& G_T \in \mathbb{R}, \underline{\mu} \in \mathbb{R}^{(nc \times np)}, \underline{n} \in \mathbb{R}_+^{(nc \times np)}, \underline{\rho} \in \mathbb{R}^{np}
\end{aligned}
\tag{1}
$$

where G_T is the total Gibbs free energy of the system, $n_{i,k}$ and $\mu_{i,k}$ the number of moles and the chemical potential, respectively, of component i in phase k, ρ_k is the number density of phase k, P_k is the pressure of phase k, nc is the number of components, and np the number of phases. Since the number of phases np is an unknown integer quantity, formulation (1) is classified as a Mixed Integer Non Linear Programming (MINLP) problem. It must be solved to global optimality to ensure that the stable solution is found.

The second approach is based on the fact that when a system is at stable equilibrium there must be no driving force to cause a net transfer of work (mechanical equilibrium), heat (thermal equilibrium), or mass (chemical equilibrium). Hence, at a stable equilibrium state, the pressure, the temperature, and the chemical potential of each component in the mixture must be the same in all equilibrium phases. However, the reverse of this statement is not necessarily true, as there may exist states where the pressure, the temperature, and the chemical potential of each component in the mixture are the same in

all phases, but where the system may be at unstable or metastable equilibrium, which would not correspond to the global minimum in the free energy. The equality of pressure, temperature, and chemical potential of the components over all phases hence mathematically correspond to the *necessary* conditions for phase equilibrium, and for the case of the *P-T* flash at the pressure P_{spec} and temperature T_{spec}, can be formulated as

$$P_{spec} = P_k\left(T_{spec}, \rho_k, n_{1,k}, \ldots, n_{nc,k}\right) \qquad \forall k = 1, \ldots, np$$

$$\mu_{i,1}\left(T_{spec}, \rho_1, n_{1,1}, \ldots, n_{nc,1}\right) = \mu_{i,k}\left(T_{spec}, \rho_k, n_{1,k}, \ldots, n_{nc,k}\right) \qquad \forall k = 2, \ldots, np$$

$$\text{and } \forall i = 1, \ldots, nc$$

$$\sum_{k=1}^{np} n_{i,k} = N_i \qquad \forall i = 1, \ldots, nc$$

$$\underline{n} \in \mathbb{R}_+^{nc \times np}, \underline{\rho} \in \mathbb{R}^{np} \qquad (2)$$

Formulation (2) is a system of $np(nc + 1)$ nonlinear equations with $np(nc + 1)$ variables which is usually solved based on the assumption that the number of phases np is known *a priori*. This form allows the coupling of the phase equilibrium problem with the rest of the equations that describe a unit operation within a process modelling environment, so this approach is often used in practice. It should be noted that both formulations (1) and (2) can also be expressed in terms of mole fractions. In this case, only $nc - 1$ mole fractions are independent of each other since their sum should be equal to one. The treatment of the phase equilibrium problem is similar for sets of specifications other than temperature and pressure. Detailed descriptions can be found in [2]-[5].

The numerical solution of the phase equilibrium problem introduces distinct challenges. Clear evidence for this is that almost all existing numerical algorithms (from simple successive substitution to sophisticated global optimization methods), and hybrid combinations of these algorithms, have been employed in an attempt to solve the problem. Several comprehensive reviews can be found in the literature [6] - [13]. Here, the focus is placed on the main sources of complexity of the problem.

Both formulations (1) and (2) are highly nonlinear. Even when the number of phases (np) is known, multiple solutions can be found for problems (1) and (2). As stated earlier, among these solutions, that corresponding to the global minimum of the total Gibbs free energy of the system is the only stable one. Undesirable solutions can either be found at local (but not global) minima of the total Gibbs free energy (referred to as metastable solutions) or, in the case of formulation (2), at maximum points of the

total Gibbs free energy. Such solutions are physically meaningless and are referred to as unstable. The degree of non-linearity and the number of solutions increase when the behavior of the mixture under consideration departs from ideality at the specified conditions. Such behavior is usually related to liquid-liquid separation, criticality, and azeotropy. In such cases the provision of a good initial guess, which drives calculations to the desired solution, becomes important.

The mathematical form of the thermodynamic model used can introduce additional complexity in the solution procedure. When equations of state (EoS) are used, the availability of analytical solutions for the vapor and liquid density roots can simplify calculations significantly. This is true for all cubic equations of state and explains their widespread use in engineering applications. Recent advances in molecular thermodynamics, however, have resulted in the development of sophisticated equations of state such as the statistical associating fluid theory (SAFT) [14, 15, 16]. Such thermodynamic approaches consist of highly nonlinear mathematical expressions which correspond to high-order polynomials (i.e. non-cubic) in terms of density that can no longer be solved explicitly in terms of density. Of particular complexity are cases in which the equilibrium phases have similar densities as in calculations of liquid-liquid equilibrium and near a critical point. In such situations, convergence can be problematic even when cubic equations of state are used.

Another source of complexity in the numerical solution of the phase equilibrium problem is the fact that the number of equilibrium phases is not known *a priori*. To overcome this complicating factor, more elaborate and multi-step algorithms have been developed based on phase stability tests that indicate whether a given solution corresponds to the global minimum of the Gibbs free energy, and if not, suggest the introduction or removal of phases before the phase equilibrium problem is solved again. The tangent plane criterion, first introduced by Gibbs [17] based on the properties of the free energy space, is the most commonly used stability test in phase equilibrium algorithms. Michelsen [18, 19] was the first to implement the tangent plane stability test within a phase equilibrium algorithm and since the tangent plane stability test involves a global search over the solution space, several authors have developed deterministic [20] - [31] or stochastic [32, 33] global search algorithms and algorithms based on continuation methods [34]. Such techniques have the advantage of converging reliably to the correct solution, although solution times can be long. Furthermore, almost all these approaches have only been applied to cubic equations

of state and activity coefficient models. Xu *et al.* [35] were the first to apply an interval Newton algorithm for the solution of the phase equilibrium and stability problems to the SAFT equation of state. The same algorithm was later applied to the construction of phase diagrams [36, 37]. Finally, Mitsos and Barton [38] have very recently proposed a reinterpretation of the Gibbs tangent plane analysis via Lagrangian duality, whereby differentiability of the Gibbs free energy is not required.

In a series of papers, we are presenting an alternative approach for the solution of the *P-T* flash problem for binary mixtures. A generic framework is proposed, which can be adapted to the needs of any equation of state of general form. The framework is based on a systematic analysis of the form and the geometrical properties of the various thermodynamic spaces involved in the solution of the phase equilibrium problem. The overall problem is decomposed into a series of sub-problems, with useful mathematical and numerical properties that facilitate their solution. In this paper (part I) the basic principles of the framework are presented in detail through its application to a non-cubic equation of state, the augmented van der Waals equation [39]–[42]. The case of binary non-azeotropic mixtures is considered as the low dimensionality of the problem allows the graphical representation of the thermodynamic spaces, which helps to illustrate the underlying concepts. In part II we present the application of this algorithm to the construction of non-azeotropic phase diagrams through a review of the types of phase behavior predicted by the augmented van der Waals equation of state. Understanding the physical and mathematical behavior of non-azeotropic binary mixtures is a very useful stepping stone for the study of azeotropic mixtures (which are discussed in part III of this series) and multicomponent systems.

2   Overview of the proposed framework

The sequence of steps in the framework is shown schematically in figure 1. The input specifications are: the temperature (T_{spec}); the pressure (P_{spec}); the total mole fraction of each component in the binary mixture (z_i, $i = 1, 2$); and the intermolecular potential parameter values (vector Θ) that characterize the mixture under consideration for a given equation of state. The output information consists of: the number of equilibrium phases (np); the mole fraction of the two components in each phase ($x_{i,k}$, $i = 1, 2$ and $k = 1, \ldots, np$); the density of each phase (ρ_k, $k = 1, \ldots, np$); and the molar fractions of each

phase (w_k, $k = 1 \ldots np$). A few key definitions are introduced first.
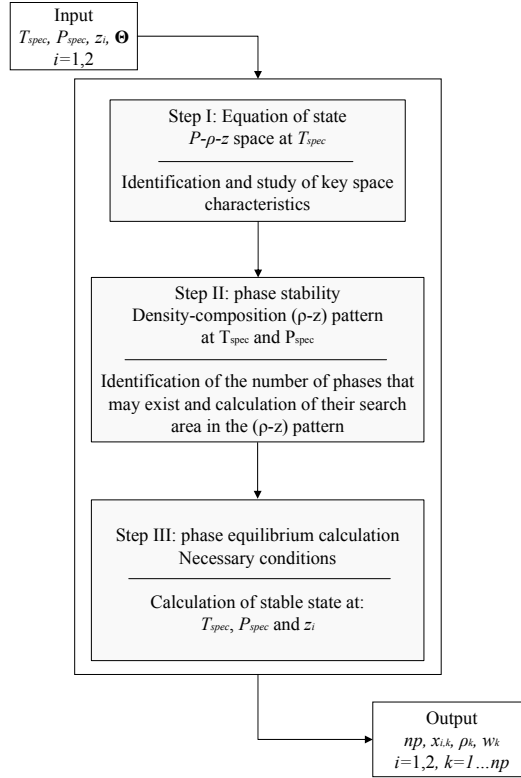

Figure 1: Overview of the framework, where P refers to the pressure, T to the temperature, ρ to the density, z to the total composition, x_i to the equilibrium mole fraction of component i, and np is the number of phases.

2.1 Key definitions

1. A *pressure-density-composition surface* is defined as the surface arising by plotting the pressure as a function of the density and composition at a fixed temperature;

2. A *density-composition pattern* is a curve or set of curves that define a cross-section of the pressure-density-composition surface along the density-composition plane at a fixed pressure;

3. A *phase* is defined to be a continuous and differentiable region on the density-composition pattern where: (i) the conditions of mechanical stability and material stability or metastability are satisfied, and (ii) there is a one-to-one mapping between density and composition.

2.2 Overview for main steps

Step I

The role of step I is to collect all the necessary information to determine the shape of the density-composition pattern at the specified temperature and pressure. The pressure-density-composition surface is thus studied at the specified temperature in step I. The mathematical properties of equations of state suggest that the pressure-density-composition surface can have only a limited number of topologies (for densities in the physical fluid range), which can be determined systematically by studying the locus of the limits of mechanical stability. Furthermore, depending on the shape of the pressure-density-composition surface, the values of pressure at certain limits of mechanical stability determine qualitative changes in the shape of the density-composition pattern. Hence, in step I, small, numerically well-behaved, problems are formulated and solved first to find the shape of the pressure-density-composition surface and subsequently to find the key pressures at which the shape of the density-composition pattern changes.

Step II

The role of step II is to determine the number of phases that may exist at the specified temperature and pressure and to identify a restricted search area for each phase in the density-composition space. First, the pressure is fixed and the shape of the density-composition pattern is determined. This is achieved by comparing the specified pressure with the key pressures calculated in step I. Due to the mathematical properties of equations of state, only a limited number of qualitatively different density-composition patterns may exist. They can be determined systematically. A series of mechanical and material stability tests are then performed on the density-composition pattern to eliminate all the unstable regions. The remaining parts of the pattern determine the existing phases (materially stable and/or metastable phases). Finally, the results of the stability tests are used to define the search area of each phase on the density-composition pattern.

Step III

In step III the stable state is found. First the necessary conditions for equilibrium (problem (2)) are applied between pairs of phases by restricting the density and the composition of each phase to lie within the search area determined in step II. The resulting formula-

tion is referred to as the "restricted necessary conditions for equilibrium," the solution of which is much easier than the full necessary conditions for equilibrium. In the case of the augmented van der Waals equation of state, studied in this work, it can be shown that the problem has at most one solution [43], which can be found reliably using a Newton-type method. The conditions for the existence of the unique solution can also be derived. Once the restricted necessary conditions for equilibrium are tested and solved for all pairs of phases, a characterization of the stable and metastable two-phase regions at the specified temperature and pressure is available. Subsequently, the metastable regions are eliminated by comparing the total Gibbs free energy of the two-phase regions which overlap in composition. As a result, the phase behavior of the system over the entire range of composition is calculated at the specified temperature and pressure. Finally, the total composition is fixed and compared with the equilibrium compositions of the multiphase regions to find the solution to the problem.

It is useful to highlight two important points relating to the proposed algorithm. Firstly, the proposed approach can be applied to any equation of state. However, since efficiency is a key issue in such calculations, any possible simplification implied by the mathematical properties of the equation of state under consideration should be taken advantage of. Such simplifications will mainly be reflected in the analysis of the pressure-density-composition surface and may reduce much of the complexity in step I. In this work, we use as an example the augmented van der Waals equation of state for mixtures, and take advantage of a number of possible simplifications as explained later. Secondly, by taking advantage of the information available at the end of each step, the proposed framework can be applied to derive information other than the solution of the phase equilibrium problem. This includes: the automated construction of temperature-composition and pressure-composition phase diagrams; the calculation of the vapor pressure and the critical point of any component which is subcritical at the specified temperature; the calculation of all the limits of mechanical and material stability of a mixture at a specified temperature and pressure; and the calculation of the properties of a phase (composition, density).

An algorithm is thus developed for binary phase equilibrium calculations for an equation of state which is complex enough to highlight the capabilities of the framework, but that is sufficiently well-structured mathematically to gain insight into the key concepts. The augmented van der Waals equation of state fits this description. It is presented with its mathematical properties in the next section.

3   The augmented van der Waals equation of state

The augmented van der Waals equation of state (AVDW EoS) [39]-[42] is based on the representation of molecules as hard spheres of volume b. The hard-sphere free volume is described by taking into account many-body interactions, as approximated by Carnahan and Starling [44], while attractions are treated at the van der Waals mean-field level in the one-fluid approximation. The equation is simple enough to facilitate the study of global phase diagrams [45], and is also accurate enough to model real systems [46].

To allow for a systematic investigation of the proposed framework in the parameter space of the augmented van der Waals equation of state, two simplifying assumptions are made: Both components are assumed to be equal-sized spheres with volume equal to 1 ($b_1 = b_2 = b = 1$), so that the terms "density" and "packing fraction" are used interchangeably in the remainder of this paper; the de Broglie wavelengths of the two components, Λ_1 and Λ_2, can be omitted from the description, since they do not affect the equilibrium compositions and densities. And to facilitate calculations further, the temperature and the pressure are scaled with respect to the energy parameter $\alpha_{2,2}$ of component 2 to yield dimensionless reduced quantities, T^* and P^*, defined as $T^* = \frac{kTb}{\alpha_{2,2}}$ and $P^* = \frac{Pb^2}{\alpha_{2,2}}$, where $\alpha_{i,j}$ denotes the binary attractive interactions between molecules of the same ($i = j$) and of different species ($i \neq j$) with respect to the interactions of 2, k is the Boltzmann constant, T the absolute temperature and P the pressure.

In this case, the reduced Helmholtz free energy, A^*, for a binary mixture of components 1 and 2 with mole fractions z_1 and z_2, respectively, can be written as

$$A^* = \frac{A}{NkT} = \left[\sum_{i=1}^{2} z_i \ln(z_i \eta) - 1 \right] + \frac{4\eta - 3\eta^2}{(1-\eta)^2} - \frac{\eta}{T^*} \sum_{i=1}^{2} \sum_{j=1}^{2} z_i z_j \frac{\alpha_{i,j}}{\alpha_{2,2}}. \tag{3}$$

Since $\alpha_{2,2}/\alpha_{2,2} = 1$ and $\alpha_{1,2} = \alpha_{2,1}$, mixtures within this equation of state are characterized by only two parameters, which are the ratios of the like $\alpha_{1,1}/\alpha_{2,2}$ and unlike $\alpha_{1,2}/\alpha_{2,2}$ attractive interactions. Without loss of generality, component 1 can be chosen to be the more volatile component. Since the two components are of equal size, this implies that $\alpha_{1,1} \leq \alpha_{2,2}$. Other thermodynamic quantities can be obtained as first or higher-order partial derivatives of the reduced Helmholtz free energy (3). The corresponding analytical expressions for the relevant derivatives are provided as supplementary material (see also [43]).

Now we discuss some of the key mathematical properties of the augmented van der Waals equation of state that are used to simplify the proposed framework.

3.1 Number of density roots of the equation of state

The pressure form of the equation of state

$$P^* = -\left(\frac{\partial A^*}{\partial V}\right)_{T^*,N} = T^* \frac{\eta + \eta^2 + \eta^3 - \eta^4}{(1-\eta)^3} - \eta^2 \sum_{i=1}^{2}\sum_{j=1}^{2} z_i z_j \frac{\alpha_{i,j}}{\alpha_{2,2}} \tag{4}$$

suggests that it corresponds to a fifth-order polynomial with respect to density, which prohibits the derivation of analytical solutions for the density roots. Analytical expressions for the density roots are readily available for all the cubic equations of state and this partly explains their widespread use in most engineering applications. However, over the last decade a shift has been apparent in the use of more sophisticated equations of state that are able to treat complex fluids more accurately. Such equations are based on a sound physical insight, but the price for this is the complexity in the corresponding mathematical expressions. The augmented van der Waals equation forms the basis of many modern equations of state.

The unavailability of analytical expressions for the density roots of the equation of state at a given pressure, temperature, composition, and set of parameters requires systematic and reliable ways to solve the pressure equation numerically. In this framework this is achieved through an exhaustive investigation of the pressure-density-composition surface in step I and subsequently the density-composition pattern in step II. An important prerequisite for this investigation is to determine the number of density roots of the equation of state within the physically allowable range of pressure, temperature, density, composition, and set of parameters. For the equation of state to be physically meaningful a maximum of three density roots should exist within the fluid density range. A proof that this is true for the AVDW equation of state is provided as supplementary material (see also [43]).

3.2 Analytical calculation of composition roots

An interesting mathematical property of the AVDW EoS, when applied to a binary mixture of equal-size molecules, is that it offers analytical expressions for the composition roots at specified temperature and pressure. This is due to the fact that this type of van der Waals one-fluid theory corresponds to a second-order polynomial with respect to composition. The corresponding expressions are of the form: $z_1 = f\left(\eta, T^*, P^*, \frac{\alpha_{1,1}}{\alpha_{2,2}}, \frac{\alpha_{1,2}}{\alpha_{2,2}}\right)$. The use of these analytical solutions can improve much the efficiency of the calculations.

However, they are not utilized in this study in order to maintain the generality of the concepts and procedures presented.

3.3 Azeotropic behaviour

Another significant simplification of the AVDW equation of state when applied to equal-size molecules is that the azeotropic composition of component 1, $x_{1,az}$, depends only on the values of the parameters of the equation of state and is given as: $x_{1,az} = (\alpha_{2,2} - \alpha_{1,2})/(\alpha_{1,1} - 2\alpha_{1,2} + \alpha_{2,2})$.

This implies that for a given mixture, the azeotropic composition is always fixed and does not depend on the temperature and pressure. The azeotropic line will thus follow the same temperature scale as the pure component vapor pressure curves.

Further investigation reveals that when $\alpha_{1,1} < \alpha_{1,2} < \alpha_{2,2}$, $x_{1,az}$ attains values outside its physical range [0,1], which implies that in this case azeotropic behavior cannot be observed; and when $\alpha_{1,2} < \alpha_{1,1} < \alpha_{2,2}$ or $\alpha_{1,1} < \alpha_{2,2} < \alpha_{1,2}$, $x_{1,az}$ attains values inside its physical range [0,1], which implies that in these cases azeotropic behavior is observed. This means that azeotropic behavior can be identified directly by comparing the values of the two parameters of the equation of state, $\alpha_{1,1}/\alpha_{2,2}$ and $\alpha_{1,2}/\alpha_{2,2}$. In addition, when non-azeotropic behavior is observed ($\alpha_{1,1} < \alpha_{1,2} < \alpha_{2,2}$), the partial derivative $\left(\frac{\partial P^*}{\partial z_1}\right)_{T,\eta}$,

$$\left(\frac{\partial P^*}{\partial z_1}\right)_{T^*,\eta} = -2\eta^2 \left(z_1 \frac{\alpha_{1,1} - \alpha_{1,2}}{\alpha_{2,2}} - z_2 \frac{\alpha_{2,2} - \alpha_{1,2}}{\alpha_{2,2}} \right), \tag{5}$$

is by inspection always seen to be positive within the physical bounds of composition. This implies that for a non-azeotropic mixture the slope of the pressure-density-composition surface at any given temperature is positive in the compositional direction. Since the focus of this papers is on non-azeotropic mixtures the case $\alpha_{1,1} < \alpha_{1,2} < \alpha_{2,2}$ will be considered.

4 Step I: The pressure-density-composition surface

In the first step of the algorithm, the temperature is fixed and the shape of the pressure-density-composition ($P^* - \eta - z_1$) surface is determined.

4.1 The shape of the pressure-density-composition surface

The shape of the $P^* - \eta - z_1$ surface is analyzed by considering any given composition and studying the shape of the corresponding projection onto the pressure-density plane. Such a projection is referred to as an isopleth. The isopleths at the boundaries of the composition range ($z_1 = 0$ and $z_1 = 1$) correspond to the pure component isotherms as described in any thermodynamics textbook (e.g. [47, 48]). Any isopleth on the interior of the composition range has similar properties to the pure component isopleths and for illustrative purposes can be considered as the isotherm of a pseudo pure component whose attractive interaction parameter is given by $\alpha = \sum_{i=1}^{2} \sum_{j=1}^{2} z_i z_j \frac{\alpha_{i,j}}{\alpha_{2,2}}$.

In the AVDW equation of state at any given pressure, an isopleth can have either one or three density roots (cf. supplementary material and [43]). An isopleth which has only one root at all pressures is supercritical, while an isopleth which has three density roots over a range of pressures is subcritical. For three roots to exist, a subcritical isopleth must exhibit an unconstrained maximum and an unconstrained minimum in pressure. These points correspond to the limits of mechanical stability, and, for a binary mixture, they satisfy:

$$\left(\frac{\partial P^*}{\partial \eta} \right)_{T^*, z_1} = 0. \tag{6}$$

For convenience, an isopleth at its critical temperature is classified as subcritical in this work. This does not restrict the applicability of the algorithm.

Furthermore, as discussed in section 3.3, for a non-azeotropic mixture, in which component 1 is the most volatile, the partial derivative $\left(\frac{\partial P^*}{\partial z_1} \right)_{T^*, \eta}$ is always positive. This implies that the slope of the $P^* - \eta - z_1$ surface remains positive in the compositional direction of component 1, and hence that the locus of an isopleth at composition $z_1 = a$ will be at higher pressures than the locus of another isopleth at composition $z_1 = b$ if $b < a$. The physical interpretation of this observation is that the pseudo pure component at composition $z_1 = a$ is more volatile than that at composition $z_1 = b$.

As a result of these mathematical properties, the $P^* - \eta - z_1$ surface for a non-azeotropic binary mixture, in which component 1 is the most volatile, can have one of the four possible shapes characterised by the topology of the loci of the limits of mechanical stability (see figures 2 to 5):

- In a type 1 surface (figure 2), all isopleths are subcritical and the locus of the limits of mechanical stability has two branches which extend over the whole composition
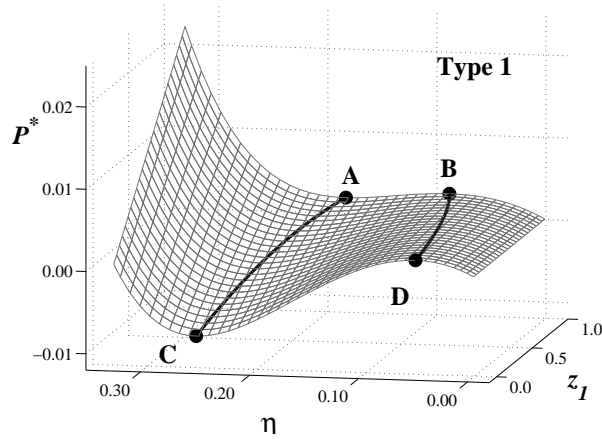
13

Figure 2: A type 1 pressure-density-composition $P^* - \eta - z_1$ surface. A, B, C, D, note the limits of mechanical stability of the pure components and the thick solid curves correspond to the locus of limits of mechanical stability for all compositions of the mixture. All isopleths are subcritical and the pressure at A is greater than the pressure at D.
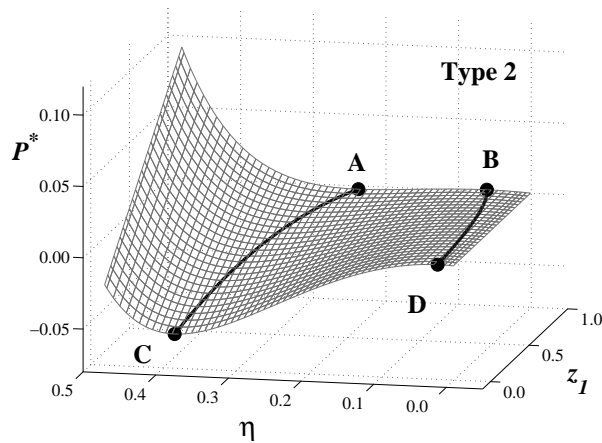

Figure 3: A type 2 pressure-density-composition surface. All isopleths are subcritical and the pressure at A is less than the pressure at D. See figure 2 for details.

range (lines A-C and B-D). Furthermore, the pressure at point A is greater than the pressure at point D.

- In a type 2 surface (figure 3), all isopleths are subcritical. The locus of the limits of mechanical stability is similar to that of type 1, but the pressure at point A is less than or equal to the pressure at point D.

- In a type 3 surface (figure 4), some isopleths are subcritical and others are super-critical. The locus of the limits of mechanical stability extends over only part of the composition space. In this case, the two branches, starting at points C and D, merge
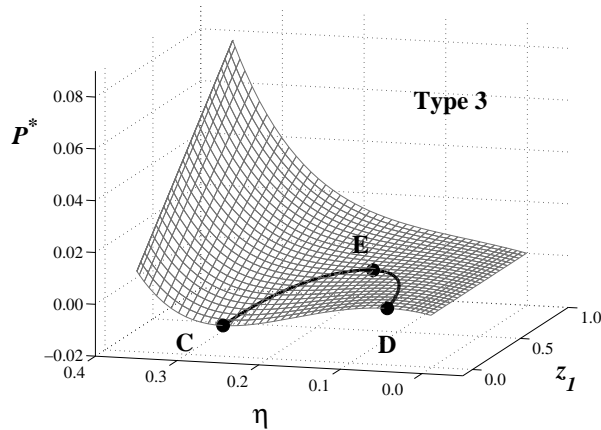
14

Figure 4: A type 3 pressure-density-composition surface. Only some isopleths are subcritical. See figure 2 for details
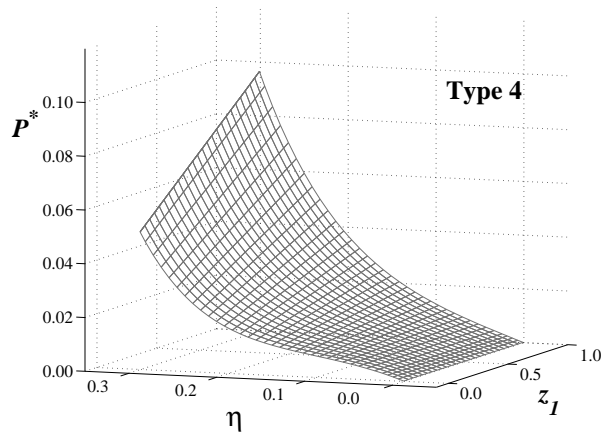

Figure 5: A type 4 pressure-density-composition surface. All isopleths are supercritical. See figure 2 for details.

at point E, the pseudo-critical point [50]. The isopleth which passes through point E has three identical density roots at that point and separates regions of subcritical and supercritical isopleths. Consequently, the following mathematical conditions hold at the pseudo-critical point (analogous to a pure component critical point):

$$\left(\frac{\partial P^*}{\partial \eta}\right)_{T^*, z_1} = 0 \quad \text{and} \quad \left(\frac{\partial^2 P^*}{\partial \eta^2}\right)_{T^*, z_1} = 0 \tag{7}$$

- In a type 4 surface (figure 5), all isopleths are supercritical and there are no limits of mechanical stability on the surface.

The classification that we use for the types of $P^* - \eta - z_1$ surfaces presented here are not related to the types of phase behavior as defined by van Konynenburg and Scott [49].
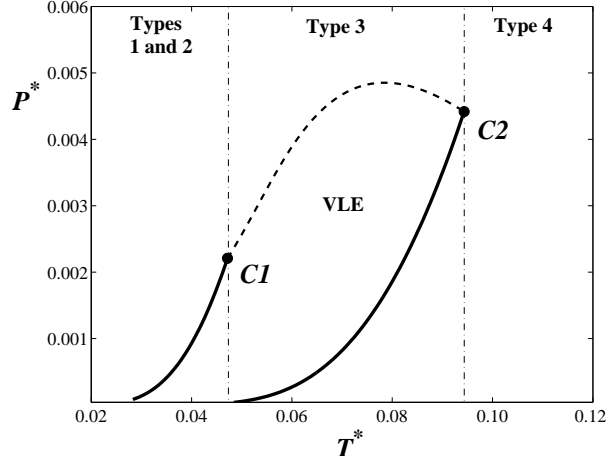
Figure 6: The P^*-T^* diagram for a binary mixture with $\alpha_{1,1}/\alpha_{2,2} = 0.5$ and $\alpha_{1,2}/\alpha_{2,2} = 0.75$. The temperature regions for which different types of $P^* - \eta - z_1$ surfaces occur are separated by dash-dotted lines. The thick solid curves correspond to the vapor pressure curves of the pure components, and the dashed curve to the locus of vapor-liquid critical points. C_1 and C_2 note the critical points of the pure components.

A physical interpretation of the four types of surfaces can be gleaned from an inspection of the temperature-pressure phase diagram shown in figure 6. For all temperatures below the critical temperature of component 1 (T^*_{C1}), both pure components are subcritical in temperature, which gives rise to $P^* - \eta - z_1$ surfaces of type 1 and/or 2. For temperatures between the critical temperatures of the pure components, only component 2 is subcritical in temperature. The corresponding surface in this case is of type 3, in which the pure component 1 isopleth is supercritical while the pure component 2 isopleth is subcritical. Finally, when the temperature is greater than the critical temperature of component 2, both components are supercritical in temperature. The $P^* - \eta - z_1$ surface is of type 4 in this case.

4.2   Sequence of calculations in step I

The conclusion from the above analysis is that the pure component isopleths provide all the necessary information to identify the shape of the $P^* - \eta - z_1$ surface. In figures 7a) and 7b), the pure component isopleths corresponding to the type 3 $P^* - \eta - z_1$ surface presented in figure 4 are shown. In this case, pure component 2 (figure 7a) is subcritical and the corresponding thermodynamic derivative $(\partial P^*/\partial \eta)_{T^*, z_1=0}$ exhibits two roots and a single minimum with a negative value (figure 7c). The roots are the densities of the two
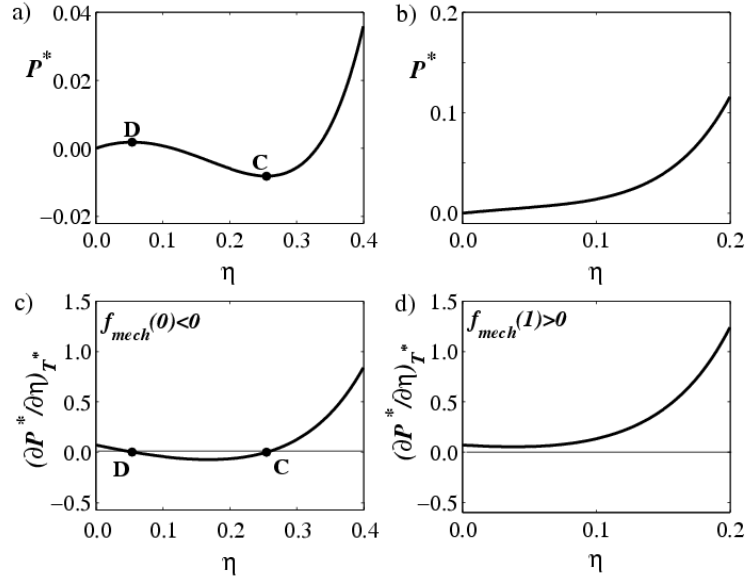
16

Figure 7: Pressure-density $P^* - \eta$ isotherms at constant composition z_1, and their corresponding derivatives with density. a) A subcritical isopleth has two limits of mechanical stability, C and D; b) a supercritical isopleth has no limits of mechanical stability; c) The derivative of the subcritical isopleth in a) has two roots and a negative minimum; d) The derivative of the isopleth in b) is always positive.

limits of mechanical stability. On the other hand, pure component 1 (figure 7b)) is supercritical and the pressure is a monotonically increasing function with respect to density so that the thermodynamic derivative $(\partial P^*/\partial \eta)_{T^*, z_1=1}$ is positive for all η (figure 7d)). Thus, in order to determine whether an isopleth $(z_1 = \hat{z}_1)$ is supercritical or subcritical, it suffices to examine whether there exists at least one value of η for which $(\partial P^*/\partial \eta)_{T^*, z_1=\hat{z}_1}$ is strictly negative. In particular, the minimum value of $(\partial P^*/\partial \eta)_{T^*, z_1=\hat{z}_1}$ can be calculated by solving the following optimization problem

$$f_{mech}(\hat{z}_1) = \min_{\eta} \quad \left(\frac{\partial P^*}{\partial \eta}\right)_{T^*, z_1=\hat{z}_1} , \quad s.t. \quad 0 \leq \eta \leq \eta_{up}, \tag{8}$$

where the upper bound η_{up} is chosen as the limit of close packing, $\pi/(3\sqrt{2})$, for a pure hard-sphere solid. If $f_{mech}(\hat{z}_1)$ is positive, then the $\hat{z}_1$ isopleth is supercritical, while if $f_{mech}(\hat{z}_1)$ is negative, then the isopleth is subcritical. In the latter case, the limits of mechanical stability can be calculated as the two roots of the partial derivative $(\partial P^*/\partial \eta)_{T^*, \hat{z}_1}=0$. To isolate the two roots, the value of the density at the solution of problem (8), $\eta_{mech}^{min}(\hat{z}_1)$, is used. The low-density root, $\eta_{mech}^{-}(\hat{z}_1)$, is smaller than $\eta_{mech}^{min}(\hat{z}_1)$ and is calculated by

solving

$$\left(\frac{\partial P^*}{\partial \eta}\right)_{T^*,\hat{z}_1} = 0, \quad 0 \le \eta \le \eta_{mech}^{min}(\hat{z}_1). \tag{9}$$

The high-density root, $\eta_{mech}^+(\hat{z}_1)$, is greater than $\eta_{mech}^{min}(\hat{z}_1)$ and is calculated by solving

$$\left(\frac{\partial P^*}{\partial \eta}\right)_{T^*,\hat{z}_1} = 0, \quad \eta_{mech}^{min}(\hat{z}_1) \le \eta \le \eta_{up}. \tag{10}$$

The pressures at the solution of problems (9) and (10) are the pressures at the limits of mechanical stability P_{mech}. The pressures at points B ($\hat{z}_1 = 1$) and D ($\hat{z}_1 = 0$) in figures 2–5 correspond to low-density roots and are given by

$$P_{mech}^-(\hat{z}_1) = P^* \left(T_{spec}^*, \eta_{mech}^-(\hat{z}_1), \hat{z}_1\right), \tag{11}$$

and the pressures at points A ($\hat{z}_1 = 1$) and C ($\hat{z}_1 = 0$) correspond to high-density roots and are given by

$$P_{mech}^+(\hat{z}_1) = P^* \left(T_{spec}^*, \eta_{mech}^+(\hat{z}_1), \hat{z}_1\right). \tag{12}$$

If both pure components are subcritical, then, by comparing the pressure at points A and D ($P_{mech}^+(\hat{z}_1 = 1)$ and $P_{mech}^-(\hat{z}_1 = 0)$, respectively), one can determine whether the $P^* - \eta - z_1$ surface is of type 1 or 2. Finally, in the case of a type 3 $P^* - \eta - z_1$ surface, the pseudo-critical pressure (point E in figure 4) is calculated by solving an optimization problem formulated as

$$P_{p-c} = \max_{\eta,z_1} \; P^*, \quad s.t. \quad \left(\frac{\partial P^*}{\partial \eta}\right)_{T^*,z_1} = 0, \quad \sum_{i=1}^{2} z_i = 1. \tag{13}$$

The density and composition at point C or D can be used as an initial guess to solve this problem reliably.

The numerical solution of each of the problems posed in step I of the algorithm is straightforward. Problem (8) is a one-dimensional problem with a unique solution as discussed in the supplementary material. Problems (9) and (10) are also one-dimensional and have unique solutions due to the use of $\eta_{mech}^{min}(\hat{z}_1)$ as a bound on the solution. Problems (11) and (12) are direct function evaluations. Finally, problem (13) is two-dimensional; it has a unique solution for a non-azeotropic mixture and the use of a feasible initial guess (point C or D) ensures robust convergence.

Table 1: Step I of the algorithm

1. Fix the temperature T^*.

2. For isopleths $\hat{z}_1 = 0$ and $\hat{z}_1 = 1$,

   - Solve problem (8).

   - If $f_{mech}(\hat{z}_1) \leq 0$, isopleth is subcritical. Solve problems (9) to (12) to obtain densities and pressures at both limits of mechanical stability. Else isopleth is supercritical.

3. (a) If both isopleths $\hat{z}_1 = 0$ and $\hat{z}_1 = 1$ are subcritical,

   - If $P^-_{mech}(\hat{z}_1 = 0) < P^+_{mech}(\hat{z}_1 = 1)$, surface is of type 1.
   - Else, surface is of type 2.

   (b) Else if isopleth $\hat{z}_1 = 0$ is subcritical and isopleth $\hat{z}_1 = 1$ is supercritical, solve problem (13) to obtain the pseudo-critical pressure. Surface is of type 3.

   (c) Else surface is of type 4.

Table 2: Characterization of the four types of $P^* - \eta - z_1$ surfaces. P_{mech} refers to the limit of mechanical stability and P_{p-c} to the pseudo-critical point; (0) denotes the $\hat{z}_1 = 0$ isopleth, and (1) the $\hat{z}_1 = 1$ isopleth.

Type	$\hat{z}_1{=}0$	$\hat{z}_1{=}1$	Limits of mechanical stability and pseudo-critical point
1	subcritical	subcritical	$P^+_{mech}(0) < P^-_{mech}(0) < P^+_{mech}(1) \leq P^-_{mech}(1)$
2	subcritical	subcritical	$P^+_{mech}(0) < P^+_{mech}(1) \leq P^-_{mech}(0) < P^-_{mech}(1)$
3	subcritical	supercritical	$P^+_{mech}(0) < P^-_{mech}(0) < P_{p-c}$
4	supercritical	supercritical	–

4.3   Summary of step I

At the end of step I (table 1), the pressures and densities at the pure component limits of mechanical stability and at the pseudo-critical point (if present) are known. The four different types of shapes of the $P^* - \eta - z_1$ surface are summarized in table 2, where the pressures of the limits of mechanical stability and of the pseudo-critical point are

presented in ascending order. All this information will be valuable in the next steps of the algorithm.

5 Step II: Phase stability – the density-composition space

In the second step of the algorithm, both the temperature and the pressure are fixed and the density-composition pattern is identified (section 5.1). For the analysis of the density-composition pattern, step II is organized into three stages (sections 5.2-5.4).

5.1 Density-composition patterns

A density-composition pattern is defined as a cross-section of the $P^* - \eta - z_1$ surface along the $\eta - z_1$ plane at the specified pressure. It therefore gives a mapping between density and composition. The possible shapes of this mapping are limited by the mathematical properties of the equation of state and the type of $P^* - \eta - z_1$ surface. There is only a restricted number of patterns which may occur. Consider, for instance, the type 1 $P^* - \eta - z_1$ surface shown in figure 8. The limit of mechanical stability with the smallest positive pressure is at point D, and that with the largest pressure is at point B (note that while it is possible to obtain metastable negative pressures, the coexistence pressure is always greater than zero, hence bounding the problem). At pressures below that of point D, the density-composition pattern consists of two detached parts, shown as a dashed curve in the figure. One part of this pattern corresponds to low values of density and extends over the whole range of compositions, while the other exhibits a loop in composition which connects to the $z_1 = 0$ isopleth at both ends and which lies in the region of intermediate to high densities. As the pressure is increased towards that of point D, the loop grows larger until it becomes attached to the low-density part of the pattern at the pressure of D. For all pressures between that of D and that of the high-density limit of mechanical stability of component 1 (point A), the pattern forms a double loop in composition as shown by the thick continuous curve in figure 8 (the orientation of the figure is such that it appears that these two pressures are equal, but in fact $P^+_{mech}(1) > P^-_{mech}(0)$ corresponding to a type 1 surface). The two end-points for this pattern lie on the two pure component isopleths, but the two turning points can be at any composition. As the pressure is increased above that of point A, the pattern separates again into two
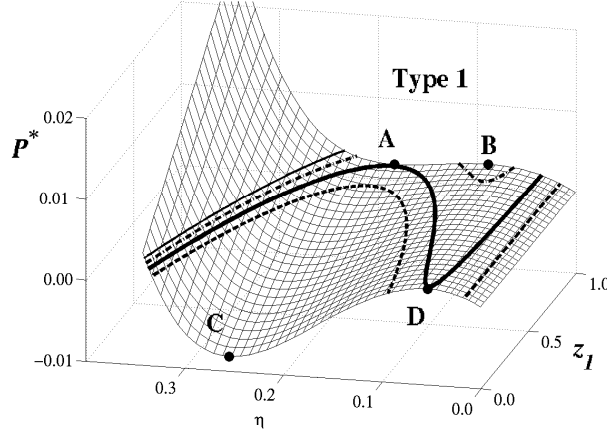
Figure 8: A type 1 $P^* - \eta - z_1$ surface, on which all four qualitatively different density-composition patterns are represented. Points A to D denote the limits of mechanical stability on the pure component isopleths and $0 > P_C^* < P_D^* < P_A^* < P_B^*$. The thick dashed curve corresponds to locus of constant pressure points for $P_C^* < P_{spec}^* < P_D^*$, the thick continuous curve to $P_D^* < P_{spec}^* < P_A^*$, the thick dashed-dotted curve to $P_A^* < P_{spec}^* < P_B^*$ and the thin continuous curve to $P_{spec}^* > P_B^*$

parts. In this case, the part which extends over the whole range of compositions is in the high-density region, while the part which exhibits the loop in composition lies at lower values of density, as shown by dash-dotted curves in figure 8. As the pressure increases from that of point A to that of the low-density limit of mechanical stability of component 1 (point B in figure 8), the low-density loop becomes smaller. It eventually disappears when the pressure reaches that of point B. Above this pressure, the pattern consists of only one high-density part that extends over the whole range of compositions as shown by a thin solid line in figure 8. In summary, only four qualitatively different patterns characterize the type 1 $P^* - \eta - z_1$ surface shown in figure 8. Other patterns can be observed by considering type 1 surfaces in which the pressure at point C is positive, or the other types of $P^* - \eta - z_1$ surfaces. Similar studies on all these cases reveal that there are only seven qualitatively different patterns that represent all possible mappings of density and composition. These are presented in figure 9.

An analysis of the patterns in figure 8 indicates that the type of pattern observed for a mixture at given temperature and pressure depends first on the type of $P^* - \eta - z_1$ surface found at the given temperature, and second on the value of the pressure relative to the key pressures calculated in step I and summarized in table 1 of the supplementary material. This analysis has been repeated for all types of $P^* - \eta - z_1$ surfaces and the

21

occurrence of the seven patterns in the four types of $P^* - \eta - z_1$ surfaces is summarized in table 3. In surfaces of types 1 and 2, patterns e and f can readily be differentiated based on whether the specified pressure is above or below the pressure of all the limits of mechanical stability, respectively. In type 3 surfaces, the value of the pressure relative to the pseudo-critical point pressure, P_{p-c}, becomes important as it marks the change in the type of density-composition pattern. In addition pattern e does not occur. In surfaces of type 4, patterns e and f are equivalent. The main conclusion from table 3 is that the relevant pattern can be identified based entirely on the results of step I and the pressure of interest.
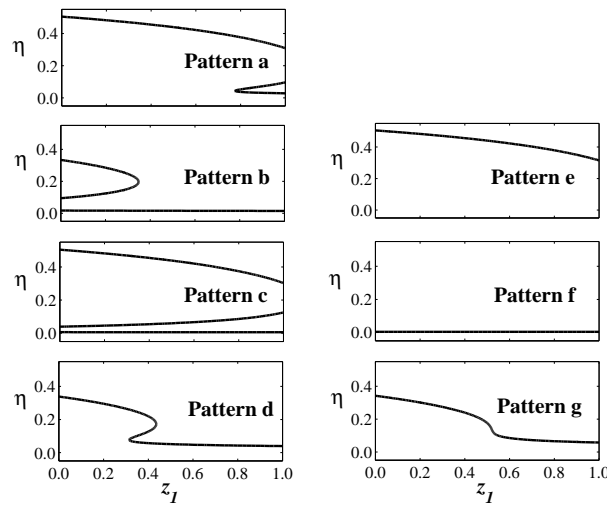

Figure 9: All seven density-composition $\eta - z_1$ patterns which can be observed in a non-azeotropic mixture.

Table 3: Conditions under which each of the seven density-composition patterns are observed. P denotes the specified pressure. All other symbols are as defined in table 2.

Pattern	Type of $P^* - \eta - z_1$ surface at the specified temperature			
	1	2	3	4
a	$P^+_{mech}(1) \leq P < P^-_{mech}(1)$	$P^-_{mech}(0) < P < P^-_{mech}(1)$	–	–
b	$P^+_{mech}(0) \leq P < P^-_{mech}(0)$	$P^+_{mech}(0) \leq P < P^+_{mech}(1)$	$P^+_{mech}(0) \leq P < P^-_{mech}(0)$	–
c	–	$P^+_{mech}(1) \leq P \leq P^-_{mech}(0)$	–	–
d	$P^-_{mech}(0) \leq P < P^+_{mech}(1)$	–	$P^-_{mech}(0) \leq P < P_{p-c}$	–
e	$P^-_{mech}(1) \leq P$	$P^-_{mech}(1) \leq P$	–	any P
f	$P < P^+_{mech}(0)$	$P < P^+_{mech}(0)$	$P < P^+_{mech}(0)$	any P
g	–	–	$P_{p-c} \leq P$	–

5.2   Step IIa: Mechanical stability – density branches

The role of the density-composition pattern is central in the overall algorithm. Equations of state are explicit functions of temperature, density and composition. However, at fixed temperature and pressure, only certain combinations of density and composition are allowed, and the density-composition pattern consists of all those possible combinations. Thus, in mathematical terms the density-composition pattern represents the feasible region of the problem. In physical terms, it also provides information on the types of phases which may be observed. In the first instance, the types of phases which may exist can be derived directly from the form of the pattern. For this purpose the concept of density branch is introduced. A density branch is a once-continuously differentiable region of the density-composition pattern over which a one-to-one mapping between density and composition exists. Based on figure 9 a pattern may therefore consist either of one branch (patterns e, f, g) or three branches (patterns a, b, c, d). This is a direct consequence of the fact that the equation of state has at most three density roots at any given temperature and pressure. A density branch that spans higher densities suggests that one or two liquid phases may exist and it is referred to as a "liquid density branch". The density and composition of any liquid phase must lie on this branch, which therefore defines the $\eta - z_1$ search area for all liquid phases. Patterns a to e have a liquid density branch. Similarly, a density branch that spans lower densities is a vapor branch and it defines the $\eta - z_1$ search area for the vapor phase. Patterns a to d and pattern f have a vapor density branch. The intermediate density branch which is observed in patterns a to d is mechanically unstable, because it is the locus of points where the thermodynamic derivative $\left(\frac{\partial P^*}{\partial \eta}\right)_{T^*,z_1}$ is negative. Mechanically unstable branches should be discarded from the phase equilibrium calculations since any density-composition combination on these branches is unstable.There are two cases in which it is not possible to identify distinct vapor and liquid branches. First, in pattern g, which occurs close to a vapor-liquid critical point, vapor and liquid phases all lie on the same mechanically stable branch. Second, for type 4 surfaces, where both components are supercritical, the concept of vapor and liquid becomes irrelevant, and patterns e and f are equivalent.

The branches of the density-composition patterns give valuable information of the possible existence of vapor and liquid phases at the specified temperature and pressure. In the particular case of the augmented van der Waals equation of state, the use of the analytical expressions for calculating the composition roots (presented in section 3.1) can

improve the performance of the algorithm at this stage. However, in order to maintain the generality of the concepts and procedures presented they are not used. An important property of patterns a to e is that the search areas for the liquid and vapor branches are distinct. For cubic equations of state, analytical expressions are available which relate density roots, and hence density branches, to the pressure, temperature, and composition. As a consequence, difficulties are only encountered when phases belong to the same density branch, such as when multiple liquid phases are present, or when the vapor and liquid phases belong to the same branch (pattern g), close to a vapor-liquid critical point. To identify the search areas for the liquid and vapor phases, the mathematical properties of patterns are further studied.

One can consider, for example, pattern b shown in figure 9(pattern b). The search areas can be defined by calculating the densities and compositions at these bounds. Since the vapor branch extends over the whole composition range, both bounds are on the pure components isopleths. Thus, only the densities need to be calculated by solving problems of the following form:

$$\text{For a given } \hat{z}_1, \text{ find } \eta \text{ such that:} P_{spec} = P^* \left(T_{spec}, \eta, \hat{z}_1 \right) \text{ and } \eta_{lo} < \eta < \eta_{up}. \qquad (14)$$

For the $\hat{z}_1 = 0$ isopleth, it is clear from figure 9 (pattern b) that three density values can be found. To make sure the value on the vapor branch is identified, the low-density limit of mechanical stability of component 2 is used as an upper bound in problem (14), that is $\eta_{up} = \eta_{mech}^-(0)$. A value of zero is used for the lower bound ($\eta_{lo} = 0$). For the $\hat{z}_1 = 1$ isopleth, the low-density limit of mechanical stability of component 1 is used as an upper bound in problem (14) to facilitate its numerical solution (i.e., $\eta_{up} = \eta_{mech}^-(1)$). Once again, zero is used as a lower bound ($\eta_{lo} = 0$). The bounds on the vapor search area obtained in this way are denoted by $z_{1,lo}^V$, $z_{1,up}^V$, η_{lo}^V, η_{up}^V, where $\eta_{lo}^V < \eta_{up}^V$. Here, $z_{1,lo}^V = 0$ and $z_{1,up}^V = 1$.

The liquid density branch in figure 9 (pattern b) extends over part of the composition range and has one bound on the pure component 2 isopleth and the other at the turning point of the composition loop. The bound on the pure component isopleth $\hat{z}_1 = 0$ is calculated by solving a problem of form (14), where the high-density limit of mechanical stability of component 2 is used as a lower bound on the solution ($\eta_{lo} = \eta_{mech}^+(0)$) to make sure the desired density is found. The upper bound is taken to be the physical bound on density ($\eta_{up} = \pi/(3\sqrt{2})$). For the other liquid branch bound, which corresponds to a turning point, the fact that the thermodynamic derivative $\left(\frac{\partial z_1}{\partial \eta} \right)_{T^*, P^*}$ is equal to zero is

24

used. This derivative is given by

$$\left(\frac{\partial z_1}{\partial \eta}\right)_{T^*, P^*} = - \left(\frac{\partial P^*}{\partial \eta}\right)_{T^*, z_1} \bigg/ \left(\frac{\partial P^*}{\partial z_1}\right)_{T^*, \eta}. \tag{15}$$

It should be noted at this point that the partial derivative $\left(\frac{\partial P^*}{\partial z_1}\right)_{T^*, \eta}$ appearing in the denominator of equation (15) can never be zero in our binary systems, as it is strictly positive for non-azeotropic mixtures. The roots of equation (15) correspond to points $\left(\frac{\partial P^*}{\partial \eta}\right)_{T^*, z_1} = 0$, which, by definition, correspond to limits of mechanical stability at the specified pressure and temperature. To calculate the density and composition at these points, a system of nonlinear equations of the following form can be solved:

$$P_{spec} = P^* \left(T_{spec}, \eta, z_1\right); \left(\frac{\partial P^*}{\partial \eta}\right)_{T^*, z_1} = 0; \sum_{i=1}^{2} z_i = 1. \tag{16}$$

Due to the shape of the $P^* - \eta - z_1$ surface, problem (16) has one solution for the particular case of pattern b. The choice of a good initial guess is very important. In pattern b, the use of the high-density limit of mechanical stability of pure component 2 (available from step I) guarantees that the last two equations in the system are satisfied, and allows Newton-based algorithms to converge. The bounds on the liquid phase search area are denoted $z_{1,lo}^L$, $z_{1,up}^L$, η_{lo}^L, and η_{up}^L, where $\eta_{lo}^L < \eta_{up}^L$, and $z_{1,lo}^L = 0$. In the case of pattern a, problem (16) has one solution as well, while two solutions exist for pattern d. The choice of an appropriate pure component limit of mechanical stability as an initial guess for the solution of problem (16) in these cases can guarantee convergence to the correct density and composition.

Using information from step I, and the analysis of the density-composition patterns, the number and type of density branches, and their bounds, can be determined following the procedure shown in table 4 (Step IIa). Furthermore, it is known that the liquid and vapor branches that exist are not mechanically unstable. In the next stages of Step II we aim to investigate further whether phases exist or not. This involves two rigorous stability tests on the branches found: one based on the vapor pressures of the pure components, and one based on material instability.

5.3 Step IIb: Mechanical stability - pure component vapor pressure test

For a non-azeotropic binary mixture, if the specified pressure is greater than the vapor pressure of the most volatile component (component 1 in this algorithm), then only liquid

phases can be stable. Similarly, if the specified pressure is less than the vapor pressure of the least volatile component (component 2 in this algorithm), then only the vapor phase can be stable. When both vapor and liquid density branches exist, it may be possible to discard one of the branches by comparing the specified pressure to the pure component vapor pressures. This can only occur for patterns a, b and c, in which gas and liquid branches are present and at least one branch extends over the whole composition range. In this case, the specified pressure and the vapor pressure of one of the pure components are in the same pressure interval as specified in table 3, because the vapor pressure of a

Table 4: Step IIa of the algorithm – Density branches and their bounds

1. Fix the pressure to the specified value P_{spec}.

2. Use table 3 to identify the relevant pattern.

3. If pattern a, b, c, d, or e, find bounds for liquid branch:

   - If pattern a, c or e, $z_{1,lo}^L = 0$, $z_{1,up}^L = 1$. Solve problem (14) with $(\hat{z}_1, \eta_{lo}, \eta_{up}) = (0, \eta_{mech}^+(0), \eta^{up})$ and with $(z_1, \eta_{lo}, \eta_{up}) = (1, \eta_{mech}^+(1), \eta^{up})$. Assign solutions to η_{lo}^L and η_{up}^L.

   - Else if pattern b or d, $z_{1,lo}^L = 0$. Solve problem (14) with $(\hat{z}_1, \eta_{lo}, \eta_{up}) = (0, \eta_{mech}^+(0), \eta^{up})$. Solve problem (16) using $(z_1, \eta) = (0, \eta_{mech}^+(0))$ as a starting point. The composition at the solution of (16) gives $z_{1,up}^L$. The densities at the solutions (14) and (16) give η_{up}^L and η_{lo}^L respectively.

4. If pattern a, b, c, d or f, find bounds for vapor branch:

   - If pattern b, c or f, $z_{1,lo}^V = 0$, $z_{1,up}^V = 1$. Solve problem (14) with $(\hat{z}_1, \eta_{lo}, \eta_{up}) = (0, 0, \eta_{mech}^-(0))$ and with $(\hat{z}_1, \eta_{lo}, \eta_{up}) = (1, 0, \eta_{mech}^-(1))$. Assign solutions to η_{lo}^V and η_{up}^V.

   - Else if pattern a or d, $z_{1,up}^V = 1$. Solve problem (14) with $(\hat{z}_1, \eta_{lo}, \eta_{up}) = (1, 0, \eta_{mech}^-(1))$. Solve problem (16) using $(z_1, \eta) = (0, \eta_{mech}^-(0))$ as a starting point. The composition at the solution of (16) gives $z_{1,lo}^V$. The densities at the solutions (14) and (16) give η_{lo}^V and η_{up}^V respectively.

5. If pattern g, $z_{1,lo}^{LV} = 0$, $z_{1,up}^{LV} = 1$. Solve problem (14) with $(\hat{z}_1, \eta_{lo}, \eta_{up}) = (0, \eta_{mech}^+(0), \eta^{up})$ and with $(\hat{z}_1, \eta_{lo}, \eta_{up}) = (1, 0, \eta^{up})$. Assign solutions to η_{up}^{LV} and η_{lo}^{LV} respectively.

pure component always lies between the pressures at the limits of mechanical stability. In table 5 we show the pressure intervals and patterns from table 3 in which the vapor pressure of pure component 1, P_1^{sat}, and the vapor pressure of pure component 2, P_2^{sat}, can be found. To calculate the vapor pressure of pure component 1 ($\hat{z}_1 = 1$), the equilibrium conditions are solved at the specified temperature:

$$
\begin{aligned}
P_1^{sat} &= P^{*V}\left(T_{spec}, \eta^V, \hat{z}_1 = 1\right) = P^{*L}\left(T_{spec}, \eta^L, \hat{z}_1 = 1\right) \\
\mu^V &\left(T_{spec}, \eta^V, \hat{z}_1 = 1\right) = \mu^L\left(T_{spec}, \eta^L, \hat{z}_1 = 1\right) \\
0 &< \eta^V < \eta_{mech}^-(1) \\
\eta_{mech}^+&(1) < \eta^L < \eta^{up}.
\end{aligned}
\tag{17}
$$

To avoid convergence to the trivial solution, bounds are placed on the densities of the two phases. The densities at the pure component limits of mechanical stability, available from step I, are chosen as bounds and their use guarantees convergence. A similar problem is solved to calculate the vapor pressure of pure component 2.

In patterns a and c, if the specified pressure is greater than the vapor pressure of component 1, the vapor branch is discarded and pattern e is used to further study the

Table 5: Pressure intervals and patterns where the vapor pressures of the two pure components can be found. See table 2 for details of symbols.

| Pattern | Type of $P^* - \eta - z_1$ surface at the specified temperature | | | |
	1	2	3	4
a	$P_{mech}^+(1) < P_1^{sat} < P_{mech}^-(1)$	$P_{mech}^-(0) < P_1^{sat} < P_{mech}^-(1)$	–	–
b	$P_{mech}^+(0) < P_2^{sat} < P_{mech}^-(0)$	$P_{mech}^+(0) < P_2^{sat} < P_{mech}^+(1)$	$P_{mech}^+(0) < P_2^{sat} < P_{mech}^-(0)$	–
c	–	$P_{mech}^+(1) < P_2^{sat} < P_1^{sat} < P_{mech}^-(0)$	–	–

Table 6: Step IIb of the algorithm – Pure component vapor-pressure test

1. If pattern a or c,

    - Calculate P_1^{sat} from problem (17).

    - If $P_1^{sat} < P_{spec}$, change pattern to pattern e.

2. If pattern b or c,

    - Calculate P_2^{sat} from problem (17).

    - If $P_2^{sat} > P_{spec}$, change pattern to pattern f.

mixture's phase behavior. Similarly, in patterns b and c, if the specified pressure is less than the vapor pressure of component 2, the liquid branch can be discarded and pattern f is used instead. This step of the algorithm is summarized in table 6.

5.4 Step IIc: Material stability test

The liquid and vapor density branches retained at this stage are mechanically stable, i.e., the thermodynamic derivative $\left(\frac{\partial P^*}{\partial \eta}\right)_{T^*, z_1}$ is always positive at any point on each branch. The branches identified are then tested in terms of material stability as defined by Rowlinson and Swinton [48]. Material instability results in liquid-liquid separation, and in vapor-liquid separation close to and at a critical point. Hence, material stability tests only need to be performed on the liquid density branches of patterns a to e (LLE) and on the single branch of pattern g (VLE and/or LLE).

The material stability test used in this algorithm is based on the thermodynamic criteria for the stability of binary mixtures as presented by Beegle *et al.* [51, 52]. According to these authors, the stability of a single-phase state can be tested by studying the sign of an appropriate thermodynamic derivative. The choice of the most suitable thermodynamic derivative depends on the problem specifications. For a binary mixture at specified temperature and pressure, the following two equivalent criteria guarantee the stability/metastability of a single-phase state [48, 53]:

$$\left(\frac{\partial^2 G}{\partial z_1^2}\right)_{T^*, P^*} > 0 \text{ or } \left(\frac{\partial \mu_1}{\partial z_1}\right)_{T^*, P^*} > 0. \tag{18}$$

A negative value of the above derivatives implies that the single-phase state is unstable at the corresponding overall composition, and the introduction of a new phase is required to make the system stable or metastable. The roots of the above derivatives are referred to as limits of material stability or spinodal points. The locus of the limits of material stability extends to the critical point of a two-phase region. As can be seen in figure 10, for any temperature at which phase separation can occur (for instance T_2^*), there exist two limits of material stability. The segment between these two limits corresponds to all unstable single liquid phase states at that temperature. This means that, at T_2^*, the thermodynamic derivative $\left(\frac{\partial \mu_1}{\partial z_1}\right)_{T^*, P^*}$ has two roots, both of which must lie on the liquid branch. When there is a single stable liquid phase, for example at temperature T_1^* on figure 10, there are no limits of material stability and the thermodynamic derivative $\left(\frac{\partial \mu_1}{\partial z_1}\right)_{T^*, P^*}$ is positive for all compositions. Plots of the chemical potential and its partial
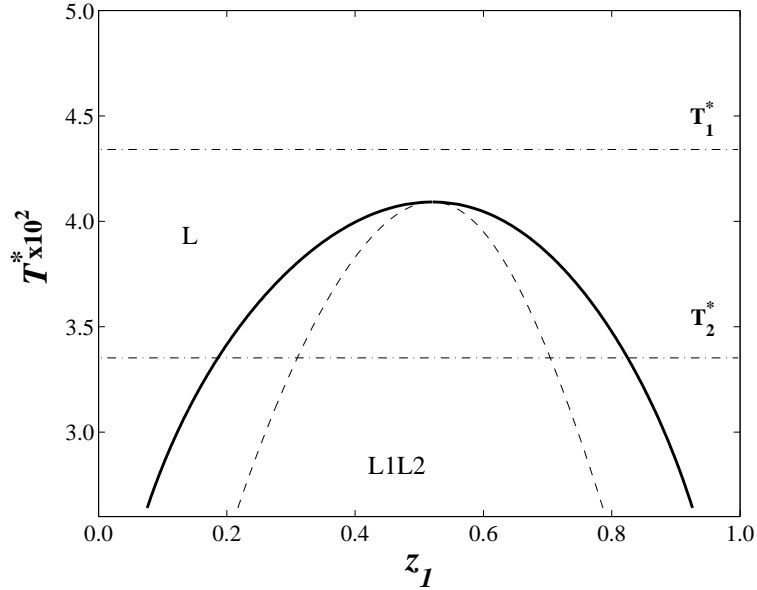
Figure 10: A constant pressure $T^* - z_1$ phase diagram showing the envelope of a liquid-liquid region (continuous curve) and the locus of the points of material stability (dashed curve).

derivative with respect to composition for these two temperatures are shown schematically in figure 11. When there is liquid-liquid separation, the chemical potential always exhibits a maximum and a minimum point at the limits of material stability (points A and B on figure 11).

On a liquid branch, only liquid-liquid separation may be detected, in which case the thermodynamic derivative $\left(\frac{\partial \mu_1}{\partial z_1}\right)_{T^*,P^*}$ has at least two roots. On the single density branch of pattern g, both vapor-liquid and liquid-liquid separation may occur, in which case there are up to four roots. Some examples that illustrate the range of behavior of $\left(\frac{\partial \mu_1}{\partial z_1}\right)_{T^*,P^*}$ when there is material instability are shown in figure 12. These cases can be described as follows:

- In figure 12a we show an example of the variation of $\left(\frac{\partial \mu_1}{\partial z_1}\right)_{T^*,P^*}$ for liquid-liquid separation when the liquid branch extends over the whole composition space (patterns a, c and e) and there exist only two roots which correspond to the limits of material stability. This is observed, for instance, in isotherm T_2^* in figure 10.

- Figure 12b corresponds to liquid-liquid separation when the liquid branch extends over part of the composition space only (patterns b and d). This may cause the appearance of a third root close to the value of z_1 at which the liquid branch terminates ($z_{1,up}^L$). The occurrence of this third root can be explained by examining the
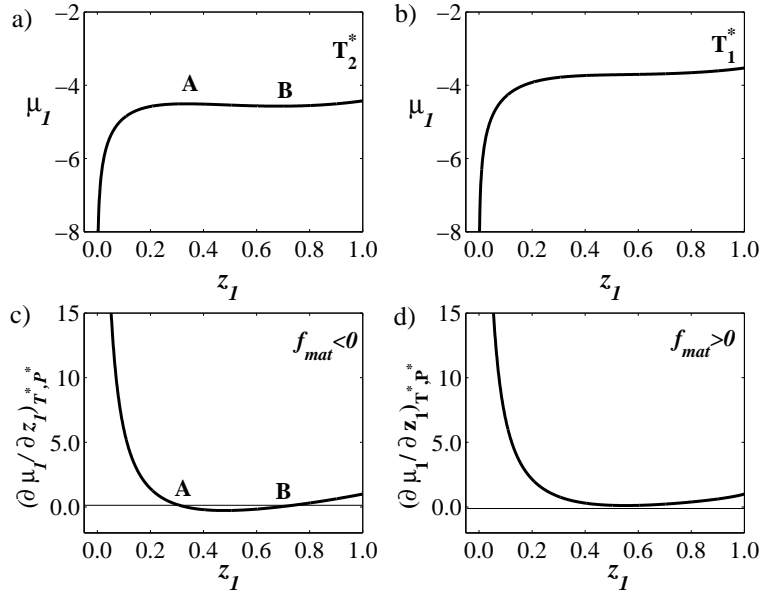
Figure 11: Chemical potential of component 1 versus mole fraction of component 1 when a) two liquid phases exist, b) one stable liquid phase exists. Derivative of the chemical potential of component 1 with respect to the mole fraction of component 1 versus mole fraction of component 1 when c) two liquid phases exist, d) one stable liquid phase exists. Points A and B in a) and c) are the limits of material stability.

Figure 12: The thermodynamic derivative $\left(\frac{\partial \mu_1}{\partial z_1}\right)_{T^*, P^*}$ as a function of z_1 when there is liquid-liquid separation: a) in patterns a, c, e; b) in patterns b, d; c) in pattern g with vapor-liquid separation; and d) in pattern g without vapor-liquid separation.

following expression for the partial derivative $\left(\frac{\partial \mu_1}{\partial z_1}\right)_{T^*,P^*}$

$$\left(\frac{\partial \mu_1}{\partial z_1}\right)_{T^*,P^*} = \left(\frac{\partial \mu_1}{\partial z_1}\right)_{T^*,\eta} + \left(\frac{\partial \mu_1}{\partial \eta}\right)_{T^*,z_1} \times \left(\frac{\partial \eta}{\partial z_1}\right)_{T^*,P^*}. \tag{19}$$
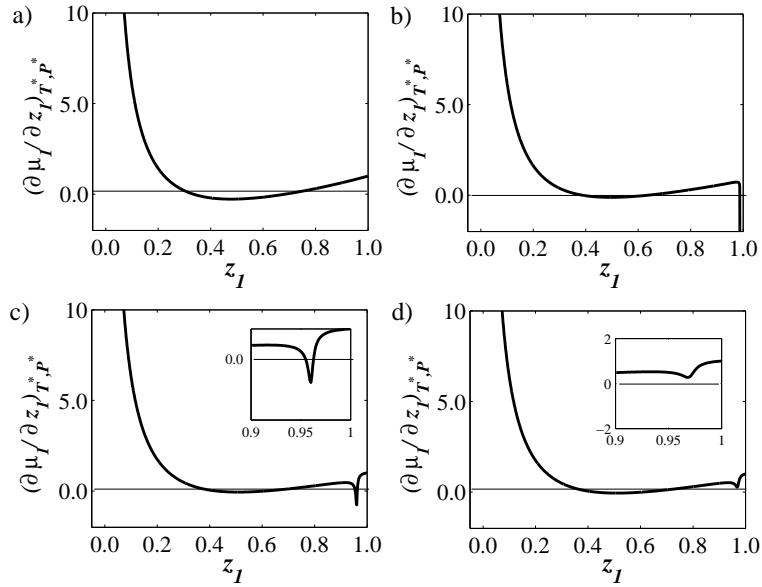
As z_1 approaches $z_{1,up}^L$ from below in patterns b and d, the partial derivative $\left(\frac{\partial \eta}{\partial z_1}\right)_{T^*,P^*}$ tends to $-\infty$, as can be seen in Figure 9. If $\left(\frac{\partial \mu_1}{\partial \eta}\right)_{T^*,z_1}$ is positive, the right-hand side of equation (19) also tends to $-\infty$, resulting in the appearance of a root near $z_{1,up}^L$. This root is often present on the liquid branch of patterns b or d. Thus, these branches have up to three roots, and liquid-liquid separation can only occur when there are two or three roots. The derivative $\left(\frac{\partial \mu_1}{\partial z_1}\right)_{T^*,P^*}$ is closely related to the determinant of the Hessian matrix of the Gibbs free energy: based on equation (18), when taken at constant temperature and pressure, the first-order derivative of μ_1 with respect to z_1 and the second-order derivative of G with respect to z_1 have the same sign. Consequently, this additional root implies the existence of regions where the Hessian matrix of the phase equilibrium problem is negative definite, which causes numerical problems for many algorithms.

- In figure 12c we show an example of the case of liquid-liquid and vapor-liquid separation due to material stability at a fixed temperature and pressure. It can be observed at elevated pressures, just below a vapor-liquid critical point (pattern g). There are four roots which correspond to the limits of material stability for the two phase separations.

- Figure 12d corresponds also to pattern g when only liquid-liquid separation occurs and hence only two roots exist. This behavior is usually seen when liquid-liquid separation occurs above a vapor-liquid critical point.

Thus, the identification of all the roots of $\left(\frac{\partial \mu_1}{\partial z_1}\right)_{T^*,P^*}$ can be used to determine whether the system exhibits material instability and hence phase separation. A related algorithm which makes use of the limits of material stability and the method of alternating tangents in determination of LLE in polymer mixtures has been presented recently [54].

Because the number of roots is not known *a priori*, global search algorithms (see for example [26, 55]) must be employed in order to guarantee a reliable investigation of phase separation. The computational cost of such methods can be high and increases quickly in the case when there are no roots at all. Due to the low dimensionality of the problem in the case of binary mixtures, an alternative approach is to
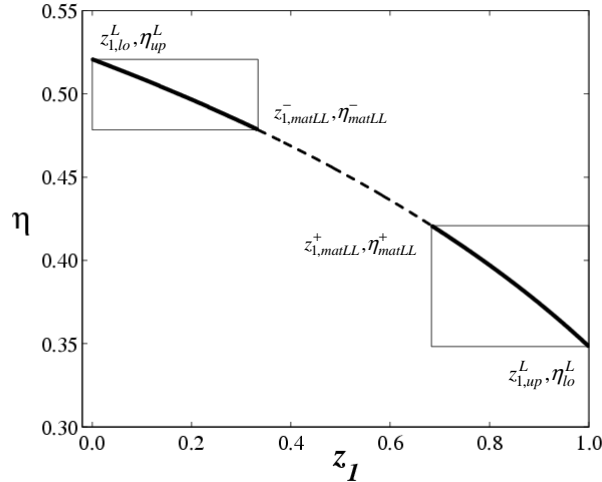
Figure 13: The liquid branch corresponding to figure 12a. The continuous curves delimit the regions of phase stability/metastability. The dashed curve denotes the region of material instability. The bounds on density and composition determined in the first two steps of the algorithm are shown. The boxes delimit the search regions to be used in subsequent steps of the algorithm.

use a path continuation method with adjustable step length, which can offer a good trade-off between efficiency and reliability [56, 57, 58]. For the specific case of the augmented van der Waals equation of state when applied to non-azeotropic mixtures, experience has shown that local search algorithms can be used reliably. In particular, a first-order liquid-liquid separation test is developed for the simplest case of patterns a, c and e (figure 12a), and a second-order test is proposed for the more complicated case of patterns b and d (figure 12b). These tests are presented as supplementary material and in [43].

If limits of material stability are found in patterns a to e, the low-composition limit is denoted by $(z_{1,matLL}^-, \eta_{matLL}^-)$ and the high-composition limit is denoted by $(z_{1,matLL}^+, \eta_{matLL}^+)$, where $z_{1,matLL}^- < z_{1,matLL}^+$. The limits of material stability give bounds on the density and composition of each of the liquid phases, as illustrated in figures 13 and 14. A liquid branch in patterns a, c and e is depicted in figure 13. The composition of liquid phase 1 is between 0 and $z_{1,matLL}^-$ and its density is between η_{matLL}^- and $\eta^L(z_1 = 0)$, where $\eta^L(z_1 = 0)$ is the liquid branch density at $z_1 = 0$ as calculated in step IIa, i.e., $\eta^L(z_1 = 0) = \eta_{lo}^L$ or η_{up}^L. Similarly, the composition of liquid phase 2 is between $z_{1,matLL}^+$ and 1, and its density between $\eta^L(z_1 = 1)$ and η_{matLL}^+, where $\eta^L(z_1 = 1)$ is the liquid branch density at $z_1 = 1$ $(\eta^L(z_1 = 1) = \eta_{lo}^L$ or $\eta_{up}^L)$. Liquid and vapor branches typical of patterns b and d are depicted in figure 14. For patterns b and d, the additional (third) root of $\left(\frac{\partial \mu_1}{\partial z_1}\right)_{T^*, P^*}$

Figure 14: A pattern of type d with liquid-liquid separation, corresponding to figure 12b. The continuous curves denote regions of phase stability/metastability on the liquid and vapor branches. The dashed curves denote the region of material or mechanical instability. The bounds on density and composition determined in the first two steps of the algorithm are shown. The area around the vapor branch is shown as an inset. The boxes delimit the search regions to be used in subsequent steps of the algorithm.

is denoted by $(z_{1,add}^L, \eta_{add}^L)$. The composition of liquid phase 1 is between 0 and $z_{1,matLL}^-$ and its density is between η_{matLL}^- and $\eta^L(z_1 = 0)$, where $\eta^L(z_1 = 0)$ is the liquid branch density at $z_1 = 0$, i.e., $\eta^L(z_1 = 0) = \eta_{lo}^L$ or η_{up}^L. The composition of liquid phase 2 is between $z_{1,matLL}^+$ and $z_{1,add}^L$, and its density between η_{add}^L and η_{matLL}^+. In the occurrence of patterns a and d, a root similar to $(z_{1,add}^L, \eta_{add}^L)$ is expected to appear in the derivative $\left(\frac{\partial \mu_1}{\partial z_1}\right)_{T^*,P^*}$ on the vapor density branch. This root is denoted by $(z_{1,add}^V, \eta_{add}^V)$, as shown in the inset of figure 14.

In pattern g, if two limits of material stability are found, the low-composition limit is denoted by $(z_{1,matLL}^-, \eta_{matLL}^-)$, and the high-composition limit by $(z_{1,matLL}^+, \eta_{matLL}^+)$. In this case, it is not possible to tell whether limits of material stability correspond to liquid-liquid or liquid-vapor separation; the subscript 'LL' is used for convenience. If four limits are found, they are denoted by $(z_{1,matLL}^-, \eta_{matLL}^-)$, $(z_{1,matLL}^+, \eta_{matLL}^+)$, $(z_{1,matLV}^-, \eta_{matLV}^-)$, $(z_{1,matLV}^+, \eta_{matLV}^+)$, in order of increasing mole fraction of component 1. Once again, these limits are physical bounds on the liquid phase and vapor phase compositions and densities. The material stability tests performed in step IIc of the algorithm are summarized in table 7.

Table 7: Step IIc of the algorithm - material stability test

1. Find all roots of $\left(\frac{\partial \mu_1}{\partial z_1}\right)_{T^*,P^*}$.

2. If pattern a, c or e,

   - If there is no root, there is a single liquid phase.

   - Else, there is liquid-liquid separation. The limits of material stability $(z_{1,matLL}^-, \eta_{matLL}^-)$ and $(z_{1,matLL}^+, \eta_{matLL}^+)$ give bounds on the two liquid phases.

3. If pattern b or d,

   - If there is one root, there is a single liquid phase.

   - Else, there may be liquid-liquid separation. The limits of material stability $(z_{1,matLL2}^-, \eta_{matLL2}^-)$ and $(z_{1,matLL2}^+, \eta_{matLL2}^+)$ and the additional root $(z_{1,add}^L, \eta_{add}^L)$ give bounds on the two liquid phases.

4. If pattern a or c, calculate root $(z_{1,add}^L, \eta_{add}^L)$ on the vapor branch

5. If pattern g,

   - If there is no root, there is no phase separation.

   - Else if there are two roots, there is one phase separation (vapor-liquid or liquid-liquid). The limits of material stability, $(z_{1,matLL}^-, \eta_{matLL}^-)$ and $(z_{1,matLL}^+, \eta_{matLL}^+)$ give bounds on the two phases.

   - Else if there are four roots, there are is vapor-liquid separation and there may be liquid-liquid separation. The limits of material stability $(z_{1,matLL}^-, \eta_{matLL}^-)$, $(z_{1,matLL}^+, \eta_{matLL}^+)$, $(z_{1,matLV}^-, \eta_{matLV}^-)$ and $(z_{1,matLV}^+, \eta_{matLV}^+)$ give bounds on the two liquid phases and the vapor phase.

5.5 Summary of step II

In step II of the algorithm both the temperature and the pressure are fixed. Based on the output information available from step I, the density-composition pattern is identified and analyzed in terms of mechanical and material stability. At the end of step II, the following information is available

1. the number and type of all materially stable or metastable phases that exist at the specified temperature and pressure. Each phase corresponds to a distinct, con-

tinuous and differentiable segment on the density-composition pattern where: (i) the conditions of mechanical stability and material stability or metastability are satisfied and (ii) there is a one-to-one mapping between density and composition;

2. the search area for each existing phase in the density-composition space (figures 13 and 14). Here, the search area of each phase is defined as a bounding box, enclosing exactly the segment mapping for that phase on the density-composition pattern. Hence, the search areas of all existing phases are also distinct on the density-composition pattern and can never overlap. All possible cases are summarized in table 1 of the supplementary material and in [43]. These search areas are used in step III of the algorithm, where a series of two-phase equilibrium problems are solved in order to reach the final stable solution; the coexistence compositions, densities, and amounts of each phase (phase fractions) are obtained.

6 Step III: Phase equilibrium calculations

6.1 The restricted necessary conditions for equilibrium

In the third step of the algorithm, given all the stable and metastable phases and their search areas: all the stable multi-phase regions are found at the specified temperature and pressure (step IIIa) and the stable state is identified at the specified temperature, pressure and total composition (step IIIb). If, at the stable state, more than one equilibrium phase exist, the corresponding phase fractions are calculated.

The solution of the two-phase equilibrium problems between the phases identified in step IIIa is of key importance. In the context of this algorithm the restricted necessary conditions for equilibrium at the specified temperature and pressure are introduced and used. The mathematical formulation of the restricted necessary conditions for equilibrium

is as follows:

$$P^{*,\alpha}\left(T_{spec}, \eta^{\alpha}, x_1^{\alpha}\right) - P_{spec} = 0$$

$$P^{*,\beta}\left(T_{spec}, \eta^{\beta}, x_1^{\beta}\right) - P_{spec} = 0$$

$$\mu_1^{\alpha}\left(T_{spec}, \eta^{\alpha}, x_1^{\alpha}\right) - \mu_1^{\beta}\left(T_{spec}, \eta^{\beta}, x_1^{\beta}\right) = 0$$

$$\mu_2^{\alpha}\left(T_{spec}, \eta^{\alpha}, x_1^{\alpha}\right) - \mu_2^{\beta}\left(T_{spec}, \eta^{\beta}, x_1^{\beta}\right) = 0$$

$$z_{1,lo}^{\alpha} < x_1^{\alpha} < z_{1,up}^{\alpha}$$

$$\eta_{lo}^{\alpha} < \eta^{\alpha} < \eta_{up}^{\alpha}$$

$$z_{1,lo}^{\beta} < x_1^{\beta} < z_{1,up}^{\beta}$$

$$\eta_{lo}^{\beta} < \eta^{\beta} < \eta_{up}^{\beta}. \tag{20}$$

where α and β are used to denote the two phases under consideration. This formulation is based on the necessary conditions for equilibrium (problem (2)), where the material balance has been removed and where the densities and the compositions are restricted to the search areas identified in step II and summarized in table **??**. A detailed analysis of the numerical and convergence properties of problem (20) is presented in [43]. There are two possible cases.

In the first case, both phases α and β belong to the same branch on the density-composition pattern. This happens when liquid-liquid equilibrium (patterns a(LL), b(LL), c(LL), d(LL), e(LL), g(LL) and g(LLV)) or vapor-liquid equilibrium close to a critical point (patterns g(LV) and g(LLV)) is considered. It can be shown [43] that when the restricted necessary conditions for equilibrium have a solution, it is unique. Furthermore, the necessary and sufficient conditions for a solution to exist have been derived [43] and can be implemented for use within the algorithm. Finally, the solution, if it exists, can thus be found from any starting point within the search area by applying a Newton algorithm.

In the second case, the two phases belong to different density branches. This happens when vapor-liquid equilibrium is considered (patterns a, b, c, and d). As in the first case, when the restricted necessary conditions for equilibrium have a solution, it is unique [43]. The existence of a solution can be readily ascertained [43]. Since in the context of this algorithm component 1 is the most volatile, and azeotropic mixtures are not considered, it can be shown that, at the solution, the composition of component 1 in the vapor phase, $x_1^{*,V}$, is always greater than the composition of the same component in the liquid phase,

$x_1^{*,L}$. When a solution exists, it can be found from any starting point at which $x_1^V > x_1^L$ by applying a Newton algorithm.

6.2 Step IIIa: Calculation of all stable multiple phase states at the specified temperature and pressure

In step IIIa the temperature and pressure are fixed to the specified values and the restricted necessary conditions for equilibrium (20) are solved between all pairs made from the phases identified in step II. It is well-known that with equations of state of the type considered here, there can only be up to three fluid phases in coexistence in a binary mixture. In the case of a non-azeotropic mixture a maximum of three phases can be identified in step II: liquid phase $L1$ which is either the default liquid phase or the liquid phase at lower composition of component 1 when liquid-liquid separation occurs; liquid phase $L2$ which corresponds to the liquid phase at higher composition of component 1 when liquid-liquid separation occurs; and the vapor phase V; so that a maximum of three pairs of phases have to be studied: $L1L2$, $L1V$ and $L2V$.

For a given pair of phases $(\alpha, \beta) \in \{L1, L2, V\}^2, \alpha \neq \beta$, the existence of a unique solution of the restricted necessary conditions for equilibrium (20) is first tested as described in [43]. If that solution exists, problem (20) is solved to find the equilibrium compositions ($x_{1,\alpha\beta}^{*,\alpha}$ and $x_{1,\alpha\beta}^{*,\beta}$) and densities ($\eta_{\alpha\beta}^{*,\alpha}$ and $\eta_{\alpha\beta}^{*,\beta}$) of the two phases. This procedure is repeated for all pairs of phases. As a result all the stable and metastable two-phase regions at the specified temperature and pressure are obtained.

Comparisons between the calculated equilibrium compositions are performed next to identify and discard any metastable two-phase regions and to locate three-phase lines. The following criteria are used:

1. if there exists a single two-phase region, it is always stable,

2. if only L1L2 and L2V exist, then they are both stable,

3. if only L1L2 and L1V exist, then L1V is stable and L1L2 is metastable,

4. if only L2V and L1V exist, then L1V is stable and L2V is metastable,

5. if there exist three two-phase regions, namely L1L2, L1V and L2V, then:

   (a) if $x_{1,L1L2}^{*,L2} < x_{1,L2V}^{*,L2}$, then the L1L2 and L2V regions are stable and the L1V region is metastable,

(b) if $x_{1,L1L2}^{*,L2} = x_{1,L2V}^{*,L2}$, then there is three-phase equilibrium L1L2V,

(c) if $x_{1,L1L2}^{*,L2} > x_{1,L2V}^{*,L2}$, then the L1V region is stable and the L1L2 and L2V regions are metastable.

The above criteria are derived based on inspection of all possible types of phase diagrams that may occur in binary mixtures of molecules with asymmetrical interactions [49]. A more systematic way to draw the above conclusions would be the following:

1. identify all the two-phase regions which intersect in terms of their composition range. For instance in case 5(c) above, the regions of L1L2, L1V and L2V will intersect;

2. find the composition interval I over which the two-phase regions identified intersect. In case 5(c): $I = [x_{1,L2V}^{*,L2}, x_{1,L1L2}^{*,L2}]$;

3. choose any total composition $z \in I$ and calculate the total Gibbs free energy for each two-phase state identified. The state with the minimum total Gibbs free energy will be the stable one.

It should be noted, however, that the latter procedure is computationally slower.

At the end of step IIIa, all stable two- or three-phase regions are identified at the specified temperature and pressure. When the algorithm is used for the construction of phase diagrams, calculations terminate at this stage for the particular temperature and pressure. When a single flash calculation is performed the algorithm proceeds to step IIIb where the specified total composition of the mixture is fixed.

6.3 Step IIIb: calculation of the stable state at the specified temperature, pressure and total composition

In step IIIb, the total composition of interest, z_i, $i = 1, 2$, is compared with the equilibrium compositions of the stable two-phase and three-phase regions identified in step IIIa. If it lies outside multiple phase regions, the mixture is in a stable one-phase state, with composition equal to the total composition. If it lies within any of the multiple phase regions identified, then the mixture separates into the corresponding number of phases. The equilibrium compositions and densities will be as calculated in step IIIa. Furthermore, the phase fractions, w_k, are calculated by solving a linear system of equations, which for

a two-phase state can be expressed as

$$\sum_{k=1}^{2} w_k x_{i,\alpha\beta}^{*,k} = z_i, \qquad \text{for } i = 1, 2. \tag{21}$$

7 Conclusions

A framework for phase equilibrium calculations using equations of state of general form has been presented. The basic principles of the framework have been discussed in detail through an application to binary non-azeotropic mixtures described by the augmented van der Waals equation of state. The overall problem is decomposed into sub-problems, each with useful mathematical and numerical properties, which can reliably and efficiently be solved to reach the final solution.

In step I, the temperature is fixed and the pressure-density-composition surface is studied. It was shown that, under the assumptions made for the augmented van der Waals equation of state, the surface can be one of four types. To identify the correct type and determine the keys points on the surface, a series of one- and two-dimensional problems is solved. Because each problem has a unique solution, local solvers can be used for efficiency.

In step II, the information from step I is used to identify the relevant density-composition pattern at the pressure (and temperature) of interest. Only seven types of pattern are found, each representing a combination of phases. A series of tests has been proposed to determine the stability or metastability of each phase. Through the use of judicious initial guesses and bounds, the tests for mechanical stability can be performed reliably. Tests are also developed for material stability. Heuristics are proposed for their solution, but deterministic techniques with guaranteed solutions can also be used if desired.

Finally, in the third step, information about the composition ranges of the phases identified in step II is used to formulate a set of restricted phase equilibrium problems. These have unique solutions and are solved with a standard local solver.

Thus, the application of the proposed framework to the augmented van der Waals equation of state has led to an algorithm that can identify the stable solution, and much additional information on stability, through the solution of a sequence of simple problems. We feel that the methodology presented in this work will provide an invaluable platform for the robust determination of the phase equilibria in more complex multicomponent fluid mixtures. The effectiveness of this approach is highlighted in detail in part II of this

paper through the construction of binary phase diagrams.

Acknowledgements

References

[1] L. E. Baker, A. C. Pierce, K. D. Luks, SPE/ODE Second Joint Symposium on Enhanced Oil Recovery, Tulsa, Oklahoma, (1981), 471.

[2] J. F. Boston, H. I. Britt, Comp. Chem. Eng., 2, (1978), 109.

[3] J. M. Prausnitz, T. F. Anderson, E. A. Green, C. A. Eckert, R. Hsieh, J. P. O'Connell, Computer calculations for multicomponent vapor-liquid and liquid-liquid equilibria, Prentice Hall, New Jersey, 1980.

[4] M. L. Michelsen, Fluid Phase Eq., 33, (1987), 13.

[5] M. L. Michelsen, Fluid Phase Eq., 158-160, (1999), 617.

[6] W. D. Seider, R. Gautam, C. W. White, ACS Symposium Series, Washinghton D.C., 1980; 124; chapterComputation of phase and chemical equilibrium: A review, 115.

[7] R. A. Heidemann, Fluid Phase Eq., 14, (1983), 55.

[8] M. O. Ohanomah, D. W. Thompson, Comp. Chem. Eng., 8, (1984), 147.

[9] M. O. Ohanomah, D. W. Thompson, Comp. Chem. Eng., 8, (1984), 157.

[10] M. O. Ohanomah, D. W. Thompson, Comp. Chem. Eng., 8, (1984), 163.

[11] D. J. Swank, J. C. Mullins, Fluid Phase Eq., 30, (1986), 101.

[12] X. Joulia, P. Maggiochi, B. Koehret, H. Paradowski, J. J. Bartuel, Fluid Phase Eq., 26, (1986), 15.

[13] Y. S. Teh, G. P. Rangaiah, Trans. IChemE, 80, (2002), 745.

[14] W. G. Chapman, K. E. Gubbins, G. Jackson, M. Radosz, Fluid Phase Eq., 52, (1989), 31.

[15] W. G. Chapman, K. E. Gubbins, G. Jackson, M. Radosz, Ind. Eng. Chem. Res., 27, (1990), 1709.

[16] E. A. Müller, K. E. Gubbins, Ind. Eng. Chem. Res., 40, (2001), 2193.

[17] J. W. Gibbs, Transanctions of Connecticut Academy, 2, (1873), 382.

[18] M. L. Michelsen, Fluid Phase Eq., 9, (1982), 1.

[19] M. L. Michelsen, Fluid Phase Eq., 9, (1982), 21.

[20] C. M. McDonald, C. A. Floudas, AIChE J., 41, (1995), 1798.

[21] C. M. McDonald, C. A. Floudas, Ind. Eng. Chem. Res., 34, (1995), 1674.

[22] C. M. McDonald, C. A. Floudas, Comp. Chem. Eng., 19, (1995), 1111.

[23] C. M. McDonald, C. A. Floudas, Comp. Chem. Eng., 21, (1997), 1.

[24] S. T. Harding, C. A. Floudas, AIChE J., 46, (2000), 1422.

[25] Y. Zhu, Z. Xu, Ind. Eng. Chem. Res., 38, (1999), 3549.

[26] J. Z. Hua, J. F. Brennecke, M. A. Stadtherr, Fluid Phase Eq., 116, (1996), 52.

[27] J. Z. Hua, J. F. Brennecke, M. A. Stadtherr, Comp. Chem. Eng., 22, (1998), 1207.

[28] J. Z. Hua, J. F. Brennecke, M. A. Stadtherr, Ind. Eng. Chem. Res., 37, (1998), 1519.

[29] S. R. Tessier, J. F. Brennecke, M. A. Stadtherr, Chem. Eng. Sci., 55, (2000), 1785.

[30] D. V. Nichita, C. D. D. Valencia, S. Gomez, Chem. Eng. Comm., 193, (2006), 1194.

[31] K. McKinnon, M. Mongeau, J. Glob. Opt., 12, (1998), 325.

[32] Y. Zhu, Z. Xu, Fluid Phase Eq., 154, (1999), 55.

[33] G. P. Rangaiah, Fluid Phase Eq., 187-188, (2001), 83.

[34] A. C. Sun, W. D. Seider, Fluid Phase Eq., 103, (1995), 213.

[35] G. Xu, J. F. Brennecke, M. A. Stadtherr, Ind. Eng. Chem. Res., 41, (2002), 938.

[36] S. P. Tan, M. Radosz, Ind. Eng. Chem. Res., 41, (2002), 3722.

[37] S. P. Tan, M. Radosz, Ind. Eng. Chem. Res., 41, (2002), 5848.

[38] A. Mitsos, P. I. Barton, AIChE Journal, 53, (2007), 2131.

[39] B. J. Alder, C. E. Hecht, J. Chem. Phys., 50, (1969), 2032.

[40] K. N. Marsh, M. L. McGlashan, C. Warr, Trans. Faraday Soc., 66, (1970), 2453.

[41] N. F. Carnahan, K. E. Starling, AIChE J., 18, (1972), 1184.

[42] G. Jackson, J. S. Rowlinson, C. A. Leng, J. Chem. Soc. - Faraday Trans., 82, (1986), 3461.

[43] A. Giovanoglou Phase equilibria and stability for equations of state of general form: algorithms and applications PhD thesis, Imperial College, London, (2007).

[44] N. F. Carnahan, K. E. Starling, J. Chem. Phys., 51, (1969), 635.

[45] L. V. Yelash, T. Kraska, Ber. Bunsen-Ges. Phys. Chem., 102, (1998), 213.

[46] J.-L. Wang, R. J. Sadus, Fluid Phase Eq., 214, (2003), 67.

[47] A. Firoozabadi, Thermodynamics of hydrocarbon reservoirs, McGraw-Hill, 1999.

[48] J. S. Rowlinson, F. L. Swinton, Liquids and liquid mixtures, Butterworths, 3rd ed., 1982.

[49] P. H. van Konynenburg, R. L. Scott, Phil. Trans., A298, (1980), 495.

[50] R. J. Topliss, D. Dimitrelis, J. M. Prausnitz, Comp. Chem. Eng., 12, (1988), 483.

[51] B. L. Beegle, M. Modell, R. C. Reid, AIChE J., 20, (1974), 1194.

[52] B. L. Beegle, M. Modell, R. C. Reid, AIChE J., 20, (1974), 1200.

[53] J. W. Tester, M. Modell, Thermodynamics and its applications, Prentice Hall, 3rd ed., 1997.

[54] N. von Solms, I. A. Kouskoumvekaki, T. Lindvig, M. L. Michelsen, G. M. Kontogeorgis, Fluid Phase Eq., 222, (2004), 87.

[55] C. D. Maranas, C. A. Floudas, J. Glob. Opt., 7, (1995), 143.

[56] D. F. Davidenko, Dokl. Akad. Nauk. SSSR, 88, (1953), 601.

[57] H. Keller, Numerical solution of bifurcation and nonlinear eigenvalue problems, Academic Press, New York, 1977.

[58] T. L. Wayburn, J. D. Seader, Comp. Chem. Eng., 11, (1987), 7.